

Deciphering the roles of environment and development in the evolution of a Late Triassic assemblage of conodont elements

Pauline Guenser[‡], Louise Souquet[‡], Sylvain Dolédec, Michele Mazza, Manuel Rigo, and Nicolas Goudemand

Abstract.—To assess evolutionary processes in deep time, it is essential to understand the roles of development and environment, both recorded through the morphological variability of fossil assemblages. Thanks to their great abundance and the high temporal resolution of their fossil record, conodont elements are ideal to address this issue. In this paper, we present the first quantitative study of a Carnian–Norian (Late Triassic) assemblage of closely related P₁ conodont elements. Using geometric morphometrics (landmarks, sliding landmarks, and elliptic Fourier analysis), we explore the main axes of phenotypic variation and relate them to classically used taxonomic characters. We show that some important taxonomic features follow laws of covariation, hence highlighting developmental constraints. Furthermore, the intraspecific variation within all considered species, either Carnian or Norian forms, is similarly restricted, emphasizing, for the first time in conodont P₁ elements, a common line of least resistance to evolution, which means that similar intrinsic (developmental) factors were acting on these taxa and likely biased the evolutionary trajectories of all these taxa in a similar way. Because the evolution between Carnian and Norian forms is known to have followed a trajectory that is significantly different from the line of least resistance, strong extrinsic pressures, such as environmental disturbances, were probably at play around the Carnian/Norian boundary to counteract the effects of these intrinsic, developmental constraints.

Pauline Guenser*, Louise Souquet, and Nicolas Goudemand. *Université Lyon, ENS de Lyon, CNRS, Université Claude Bernard Lyon 1, Institut de Génomique Fonctionnelle de Lyon, UMR 5242, 46 Allée d'Italie, F-69364 Lyon Cedex 07, France. E-mail: louise.souquet@ens-lyon.fr, nicolas.goudemand@ens-lyon.fr. *Present address: Université Lyon, CNRS, Université Claude Bernard Lyon 1, Laboratoire d'Écologie des Hydrosystèmes Naturels et Anthropisés, UMR 5023, 3-6 rue Raphaël Dubois–Bâtiments Forel, 69622 Villeurbanne Cedex 43, France. E-mail: pauline.guenser@univ-lyon1.fr*

Sylvain Doledec. *Université Lyon, CNRS, Université Claude Bernard Lyon 1, Laboratoire d'Écologie des Hydrosystèmes Naturels et Anthropisés, UMR 5023, 3-6 rue Raphaël Dubois–Bâtiments Forel, 69622 Villeurbanne Cedex 43, France. E-mail: sylvain.doledec@univ-lyon1.fr*

Michele Mazza. *c/o Dipartimento di Scienze Chimiche e Geologiche, Università degli Studi di Modena e Reggio Emilia, via Campi 103, I-41125 Modena, Italy. E-mail: michele.mza@gmail.com*

Manuel Rigo. *IGG-CNR, Via G. Gradenigo 6, 35131 Padova, Italy. E-mail: manuel.rigo@unipd.it*

Accepted: 9 April 2019

First published online: 16 May 2019

[‡]These authors contributed equally to this work.

Data available from the Dryad Digital Repository: <https://doi.org/10.5061/dryad.m48h8ht>

Introduction

Since the dawn of modern evolutionary synthesis (Huxley 1942), macroevolution in deep time has often been considered as resulting mainly from the effects of extrinsic (environmental) factors such as climate change. In addition, random genetic mutations have been thought to produce isotropic variation upon which natural selection acts as a filter, driving the survivors toward fitness peaks (Mayr 1982; Wright 1982; Wainwright 2007; Condamine et al. 2013). Yet the question of the relative role of intrinsic (e.g.,

developmental) factors in macroevolution remains scarcely addressed (Erwin 2017; Jablonski 2017). Organisms and their shapes are constrained by the universal rules of chemistry, physics, and geometry. The set of theoretically possible forms is thus bounded by the way these forms are generated during ontogeny. In other words, developmental processes determine the variation of individuals anisotropically, thus possibly biasing evolution along favorable paths.

Because organisms and environment “actively co-determine each other” (Levins

and Lewontin 1985: p. 89), the dichotomy between intrinsic and extrinsic factors is necessarily reductive, and we should expect that explanatory schemes will involve both types of factors. Schluter (1996) first proposed that the main direction of genetic variance (termed *Gmax*) within a population corresponds to a “line of least resistance” to evolution, that is, evolution will occur more easily, and thus more frequently, in that direction rather than in any other. Interestingly, as phenotypic and genetic variance–covariance matrices are correlated (Siahsarvie 2012), the main direction of phenotypic variance (*Pmax*) is aligned with *Gmax*. The theory of lines of least resistance can thus be extended to the phenotypic variance of a population, extant or fossil (in which case, we prefer the term “assemblage”). Moreover, phenotypes do not contain information only about the development of the individuals, but also about their environment. Hence, this theoretical framework can be used to assess the relative roles of environmental and developmental processes in evolution via the analysis of the main directions of phenotypic variance in fossil assemblages (Renaud et al. 2006; Hunt 2007). The *Pmax* can be interpreted in terms of genetic/developmental constraints, and any significant deviation from *Pmax* can be interpreted as being the consequence of an environmental disturbance. To conduct such studies in deep time, one needs a framework with a fossil record that spans a large time frame and comprises large assemblages that are available at a temporal resolution that compares with the dynamics of paleoenvironmental fluctuations. Conodonts fit these requirements.

Conodonts are a group of extinct, jawless marine organisms that are considered vertebrates (Donoghue et al. 2000). They are mainly known in the fossil record by their tiny, apatitic teeth-like feeding elements. Their feeding apparatus usually includes 15 elements. The anteriorly located group of so-called S and M elements was likely used to grasp food (Goudemand et al. 2011), and in the posterior part of the mouth, two pairs of so-called P elements were used to process the food (Purnell 1994; Martínez-Pérez et al. 2016). Throughout their 300 Myr of existence (from the late Cambrian to the Late

Triassic), conodonts have one of the best spatio-temporally resolved fossil record and are often used as index fossils for relative dating of sediments and stratigraphic correlation between geological sites. Because conodont elements are also used for geochemistry-based reconstructions of paleoenvironments (Wenzel et al. 2000; Joachimski et al. 2002, 2006; Trotter et al. 2008; Sun et al. 2012), they are an ideal model system for deep-time evolutionary studies. However, until recently, conodonts were used almost exclusively in an “utilitarian” way (for biostratigraphy and paleoenvironmental reconstructions), and despite their huge potential, they have remained relatively underexploited for evolutionary studies, and virtually nothing is known about functional or developmental constraints in conodonts (Purnell 1994; Donoghue and Purnell 1999; Girard et al. 2004b; Girard and Renaud 2007; Goudemand et al. 2011; Murdock et al. 2013; Martínez-Pérez et al. 2014a, b, 2016). Qualitative descriptions of conodont element variation are ubiquitous in the literature, as they are standard in conodont systematics. Yet these descriptions are usually restricted to given species, they rarely focus on patterns of covariation, and the lack of quantification implies that they cannot be statistically evaluated.

Quantitative studies on conodont elements are made difficult by their lifelong accretionary mode of growth (Donoghue 1998): growth lamellae are periodically added around the elements, resulting in an increase of the number of denticles and a modification of the length: height ratio of the element during ontogeny, thereby hindering definition and identification of homologous landmarks and complicating biologically relevant comparisons (Jones et al. 2009). Previous quantitative analyses on conodont elements were based on classical and/or geometric morphometrics and quantified interspecific (Croll et al. 1982; Murphy and Cebecioğlu 1984; Klapper and Foster 1993; Girard et al. 2004a; Chen et al. 2009; Girard and Renaud 2011) or intraspecific variation (Murphy and Springer 1989; Ritter 1989; Jones et al. 2009; Chen et al. 2016). Some authors further described evolutionary trends (Barnett 1972; Roghi et al. 1995; Girard and Renaud 2007; Jones 2009) or linked some morphological evolutions to paleoenvironmental changes (Barnett

1972; Renaud and Girard 1999; Girard et al. 2004b; Girard and Renaud 2008), paleobiogeography (Tolmacheva and Löfgren 2000), or functional aspects (Purnell 1994; Martínez-Pérez et al. 2014a, b, 2016). For instance, Croll and coworkers (1982) used biometry (length of different parts of the element, angle measurements for denticle inclination, and curvature of the element) to describe the P₁ elements of *Ozarkodina*, *Pryantodina*, *Carniodus*, *Microzarkodina*, and *Pterospathodus* and concluded that biometry could be used for classification and identification. Renaud and Girard (1999) studied the response of *Icriodus* and *Palmatolepis* to Late Devonian extreme paleoenvironmental perturbations in terms of the P₁ element's oral outline, showing that the response of the two genera differed in time, which the authors interpreted as different sensitivities to the environmental disturbance and, hence, possibly different habitat preferences. Jones (2009) used biometry and outline analyses on Silurian material of *Pterospathodus* to test for morphological temporal trends and observed that they involved mainly allometric repatterning. Yet, so far, no study has focused on patterns of covariation between different traits of a given element to investigate developmental constraints and putative evolutionary paths of least resistance within the conodont morphospace.

Here we study the morphological variation around the Carnian/Norian boundary (CNB, Late Triassic, ca. 227 Ma) of P₁ elements from the Pizzo Mondello section (Sicily, Italy) (Mazza et al. 2012b) with geometric morphometrics. These conodont elements belong to four genera and seven species: *Carnepigondolella pseudodiebeli* and *Carnepigondolella zoeae*; *Hayashiella tuovalica*; *Epigondolella quadrata*, *Epigondolella rigoi*, and *Epigondolella uniformis*; and *Metapolygnathus communisti*. The material corresponds to a time interval that directly follows the Carnian pluvial episode (Julian/Tuvanian boundary crisis, 234–230 Ma), which was marked not only by a conodont extinction (Rigo et al. 2007), but also by major floral and faunal turnovers (Simms and Ruffell 1990; Hallam 1996; Roghi et al. 2010). The corresponding species illustrate one of the last documented conodont evolutionary radiations before their

final demise at the Triassic/Jurassic boundary (201.3 Ma) (Pálfy et al. 2007; Mazza et al. 2012b; Mazza and Martínez-Pérez 2015). This material was selected because of its excellent preservation, the relative abundance of elements in each sample/species, and the fact that it has been already the subject of extensive sampling (this section is a candidate for the GSSP of the base of the Norian [Nicora et al. 2007]) and several in-depth analyses, including a cladistic analysis (Mazza et al. 2012a), paleoenvironmental reconstructions (Muttoni et al. 2004; Mazza et al. 2010), and several ontogenetic series reconstructions in particular using synchrotron imaging (Mazza and Martínez-Pérez 2015). Ancestor–descendant relationships were also hypothesized between most of the species present in the Pizzo Mondello section. Concerning the studied data set (five genera), two lineages can be recognized, with the genus *Paragondolella* as their presumed common ancestor. Note that alternative systematics and associated phylogenetic and ancestor–descendant relationship hypotheses have been proposed for a similar conodont assemblage from Black Bear Ridge, British Columbia, Canada (Orchard 2013, 2014). Yet these hypotheses are based on a phenetic analysis and have not been tested quantitatively.

Mosher (1968) and, later, Mazza and coworkers (2012b) have already proposed hypotheses of putative evolutionary trends based on these taxa during the CNB interval. They suggested the derivation of *Metapolygnathus* and *Epigondolella* from the polyphyletic genus *Carnepigondolella*, through a series of newly derived characters: (1) the shifting of the pit, (2) the shortening of the platform, (3) the shortening of the anterior trough margin, (4) modifications of the lower margin profile of the platform, (5) the appearance of a stronger platform ornamentation (evolution of *Carnepigondolella* into *Epigondolella*), and (6) modifications of the size and relative location of the cusp. Trends 1, 2, 3, and 5 have also been described in Black Bear Ridge (Orchard 2014) for the lineages crossing the CNB (see Rigo et al. [2018] for a discussion).

In this work, we analyze the quantitative morphological variation of P₁ conodont elements within and between these seven

morphospecies and their evolution within 7 Myr around the CNB. We focus on the exploration of this data set for recurrent patterns, especially patterns of variation and covariation between traits.

Materials and Methods

The samples are housed in the collections of the Dipartimento di Scienze della Terra “A. Desio” (Università degli Studi di Milano). All samples are from the Pizzo Mondello section in the Sicani Mountains, western Sicily, Italy (Mazza et al. 2012b); they are dated between the latest Carnian and the earliest Norian. Conodonts from this section have an average color alteration index (CAI) of 1–1.5, indicating minimal postdepositional heating (Epstein et al. 1977; Nicora et al. 2007). The specimens were selected to be as complete as possible. A set of 8 to 24 P₁ elements per species were 3D scanned, a total of 132 P₁ elements were considered (Table 1). According to the time calibration (Kent et al. 2017: Fig. 7), the assemblage spreads over 7 Myr (230.5–222 Ma).

Based on the cladistic analysis by Mazza et al. (2012a) (Fig. 1), the five genera considered here are closely related. In particular, *Metapolygnathus* is closest to *C. zoeae*, whereas *Epigondolella* is closest to *C. pseudodiebeli*. The affinity of *Hayashiella* remains unclear. These authors also hypothesized that both *Metapolygnathus* and *Epigondolella* would derive from the paraphyletic genus *Carnepigondolella*. Note that *Epigondolella* is considered as polyphyletic since the discovery of evolutionary convergences within this genus (Mazza and Martínez-Pérez 2016). Furthermore, more recent studies on the phylogeny and evolution of the metapolygnathids (Mazza et al. 2018) led to the hypothesis that the lineage *Metapolygnathus praecomunistici*–*Metapolygnathus dylani*–*Metapolygnathus parvus* is probably phylogenetically closer to the paragondolellids than it is to the carnepigondolellids; whereas the more ornate metapolygnathids (i.e., *Metapolygnathus mersinensis* and *Metapolygnathus mazzai*) would be more closely related to *Carnepigondolella*. This new interpretation, however, is compatible with the results provided by the previous cladistic analysis. The phylogenetic revision of *Epigondolella*

does not affect its relationship with *Carnepigondolella*. *Paragondolella polygnathiformis* and *Paragondolella praelindae* were the last two conodont species of *Paragondolella* to survive the Julian/Tuvalian boundary crisis caused by the Carnian pluvial episode. This genus is considered as the last common ancestor of *Norigondolella*, *Carnepigondolella*, *Epigondolella*, and *Metapolygnathus*. More precisely, *P. praelindae* is considered the ancestor of the genus *Norigondolella*, whereas *Paragondolella noah* is the ancestor of the genus *Carnepigondolella* (Mazza et al. 2012a).

To best represent the overall morphological variation of conodont elements at Pizzo Mondello, as well as to seek further support for the pattern observed with the seven studied species (see “Results”), the holotypes of species of *Paragondolella*, *Carnepigondolella*, *Metapolygnathus*, *Hayashiella*, and *Epigondolella* present in the phylogenetic analysis were also considered in this study. When good enough illustrations of the holotypes, paratypes or lectotypes were not available, well-preserved representative specimens were chosen from the literature related to the Pizzo Mondello section (Table 2).

In total, 162 conodont P₁ elements were used for this study: 132 original specimens and 30 specimens illustrated in the literature with scanning electron microscopy (SEM) images.

Digitization.—All elements were glued on wooden sticks using gum arabic and 3D scanned at 1 μm resolution using the X-ray microtomograph nanotomS (General Electric) of the AniRA-ImmOs platform, SFR Biosciences (UMS 3444), Ecole Normale Supérieure de Lyon, France. Using this technique, multiple elements could be scanned at the same time. The 3D reconstructions of the elements were obtained on Amira[®] software (v. 6.3.0), and snapshots of the elements were recorded in the standardized caudolateral, oral, and aboral views (Fig. 2). The nomenclature used in this study follows Purnell and collaborators (2000). Besides the fact that this 3D-scanning process is as fast as standard SEM imaging, one advantage of 3D scanning is that the standard views can be adjusted more easily. For comparison purposes, the morphological difference between dextral-mirrored and sinistral elements was statistically tested (see “Results”),

TABLE 1. List of the studied material: specific determination, age, stratigraphic location (sample number), number of specimens, and ontogenetic stage (sensu Mazza and Martínez-Pérez 2015). As *H. tuvalica* was not included in that study, the corresponding ontogenetic stages were determined after the illustrations of Mazza et al. (2012a: Plate 3, Figs. 3–10).

Species	Age	Sample number	Number of elements	Ontogenetic stage
<i>Hayashiella tuvalica</i>	Late Carnian	NA15	23	GS4 to GS6
<i>Carnepigondolella zoeae</i>	Late Carnian	NA15	22	GS4, GS5
<i>Carnepigondolella pseudodiebeli</i>	Late Carnian	NA15a	9	GS4, GS5
		NA16	4	GS4, GS5
		PM11a	7	GS4, GS5
		NA37	24	GS4 to GS6
<i>Metapolygnathus communisti</i>	Carnian/Norian boundary interval	NA37	24	GS4 to GS6
<i>Epigondolella uniformis</i>	Earliest Norian	NA42	8	GS4, GS5
<i>Epigondolella rigoi</i>	Early Norian	NA59	21	GS4, GS5
<i>Epigondolella quadrata</i>	Early Norian	NA60	14	GS4 to GS6

and all dextral elements (sensu Purnell et al. 2000) were mirrored into sinistral elements to avoid morphological bias induced by the bilateral symmetry (Girard and Renaud 2008).

Geometric Morphometrics.—A set of six landmarks was digitized on the aboral view, as well as a 20-sliding-landmark-based curve on the lower margin in lateral view, using tpsDig v. 2.30 (Rohlf and Marcus 1993; Rohlf 2006) (Fig. 2B). For each data set, a generalized Procrustes analysis was performed using tpsRelw v. 1.67 (Rohlf 2007). Using this method, configurations of landmarks and sliding landmarks were (1) scaled, (2) translated, and (3) rotated to minimize the sum of squared distances between corresponding landmarks. The resulting coordinates were used as shape variables for the multivariate analyses.

The outline of the element in oral view was extracted and reduced to 24 equally spaced points (origin set at the rostral geniculation point), which were used as input for an elliptic Fourier analysis (Kuhl and Giardina 1982) using the ‘Momocs’ package (Bonhomme et al. 2014) in R software (R Core Team 2018). This method decomposes the outline signal into harmonics, each described by four Fourier coefficients. Here, eight harmonics were retained, which together describe 99% of the original outlines.

The potential measurement bias introduced by slightly different orientations of the pictured elements was tested, and it was found to be not significant in this study.

The three sets of variables (landmark and sliding-landmark coordinates and coefficients of outline harmonics) were summarized using

principal component analysis (PCA) on variance–covariance matrices. Then the relationships between the three data sets were investigated using the STATIS method (Lavit et al. 1994), which allows performing the joint analysis of K tables (one per data set, $K = 3$ in our case) sharing the same rows (specimens). The STATIS method is carried out in two steps (Thioulouse and Chessel 1987; Blanc et al. 1998). In the first step, called interstructure analysis, one searches for a compromise structure computed as the weighted sum of the K tables. Coefficients are obtained from the singular-value decomposition of the matrix of the RV coefficient, which is the multidimensional equivalent of the ordinary correlation coefficient between two variables (Robert and Escoufier 1976). The corresponding eigen analysis yields factorial axes that describe the common structure across sets of variables, which is analogous to an average morphospace. During the second step, called intrastructure analysis, the projections of rows and columns of each individual data set onto the compromise axes are computed as supplementary individuals and supplementary variables, respectively. In addition, the axes of separate PCAs in each data set can be projected onto the compromise structure too, allowing for the identification of the axes of the separate PCAs best describing the common structure among the three data sets. These PCA axes are then used as shape variables. This procedure helps to minimize the number of relevant variables used in further statistical analyses. For each view, only the PCA axes that together explain at least 80% of the cumulated variance were

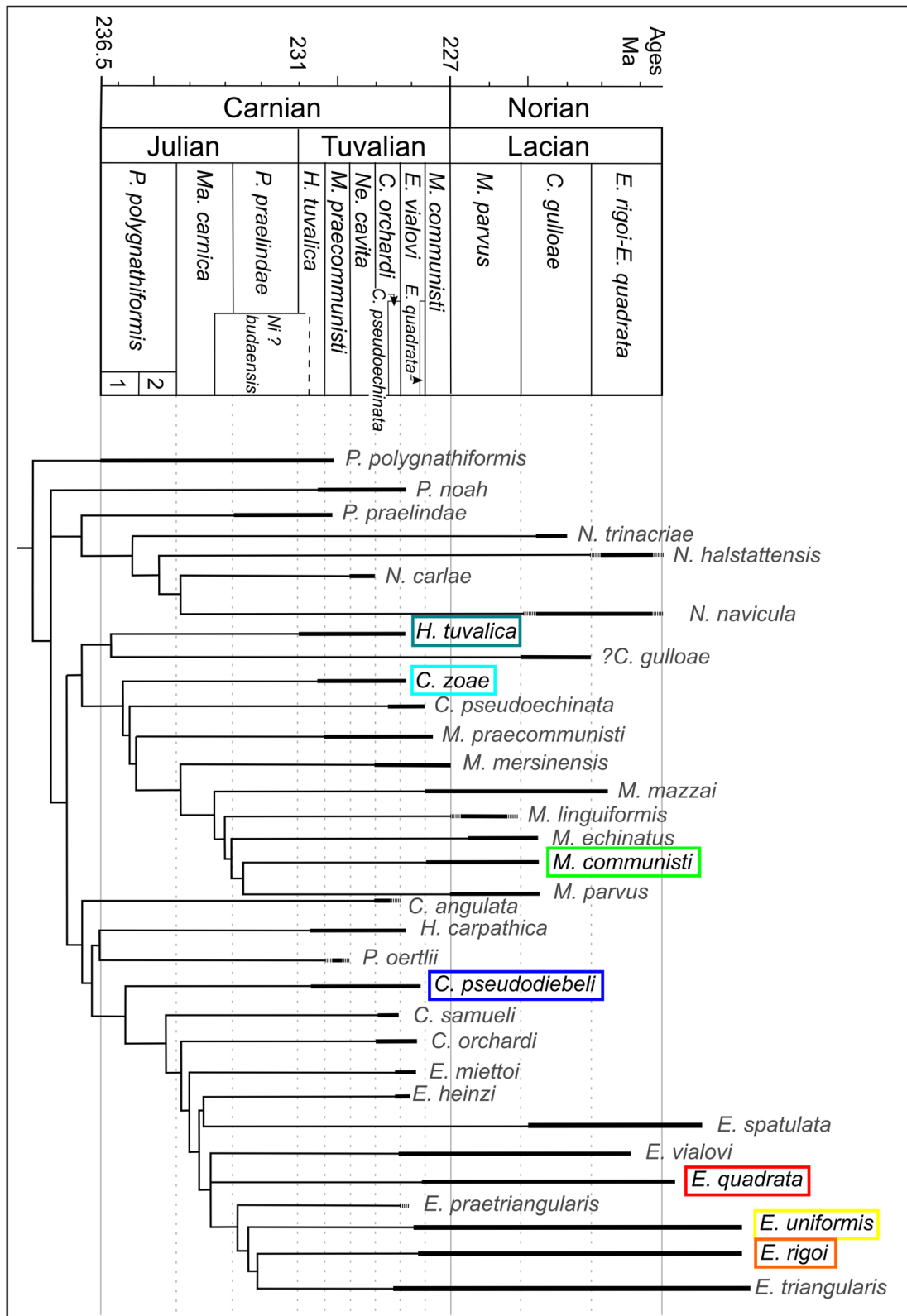


FIGURE 1. Simplified, stratigraphically calibrated, global strict consensus tree topology (modified after Mazza et al. [2012b] for the cladogram, after Rigo et al. [2018] for the species ranges and the biozonation); *C.*, *Carnepigondolella*; *E.*, *Epigondolella*; *H.*, *Hayashiella*; *Ma.*, *Mazzaella*; *M.*, *Metapolygnathus*; *Ne.*, *Neogondolella*; *Ni.*?, *Nicorraella*?; *P.*, *Paragondolella*. The taxonomy has been modified according to recent updates (after 2012), and the range of species absent (Rigo et al. 2018) are represented by dashed lines. *Hayashiella tuvalica* includes the Tuvanian forms of *Carnepigondolella nodosa* that were included in the Mazza et al. (2012b) phylogenetic study. The species considered in this study are written with black text and highlighted by a colored box drawn around them.

TABLE 2. List of holotypes or representative specimens of each species present in the phylogenetic hypothesis in Mazza et al. (2012a) considered in the data set, their corresponding numbers in Figure 4C, and the reference for each image. *Norigondolella* was not included, because it belongs to a third lineage that was not the scope of the present study.

Species and number in Fig. 4C in this paper	Nature	Source
<i>Carnepigondolella angulata</i> (1)	Holotype	Mazza et al. 2012b: Fig. 9A
<i>Carnepigondolella gulloae</i> (2)	Holotype	Mazza et al. 2012b: Plate 4, Fig. 4a–c
<i>Carnepigondolella nodosa</i> (3)	Mature growth stage	Mazza et al. 2012b: Plate 2, Fig. 4a–c
<i>Carnepigondolella orchardi</i> (6)	Mature growth stage	Mazza et al. 2012b: Plate 2, Fig. 2a–c
<i>Carnepigondolella pseudodiebeli</i> (4)	Mature growth stage	Mazza et al. 2012a: Plate 2, Fig. 8
<i>Carnepigondolella pseudoechinata</i> (5)	Mature growth stage	Balini et al. 2010: Plate 2, Fig. 6
<i>Carnepigondolella samueli</i> (7)	Holotype	Orchard 1991: Plate 1, Figs. 10–12
<i>Carnepigondolella zoeae</i> (8)	Holotype	Orchard 1991: Plate 1, Figs. 7–9
<i>Epigondolella heinzi</i> (9)	Holotype	Mazza et al. 2012b: Fig. 9C
<i>Epigondolella miettoi</i> (10)	Holotype	Mazza et al. 2012b: Fig. 9F
<i>Epigondolella praetriangularis</i> (11)	Holotype	Moix et al. 2007: Plate 1, Figs. 9,10
<i>Epigondolella quadrata</i> (12)	Holotype	Orchard 1991: Plate 2, Figs. 1–3
<i>Epigondolella rigoi</i> (13)	Holotype	Noyan and Kozur 2007: Fig. 6.4
<i>Epigondolella spatulata</i> (14)	Mature growth stage	Mazza et al. 2010: Plate III, Fig. 6a–c
<i>Epigondolella triangularis</i> (15)	Mature growth stage	Balini et al. 2010: Plate 4, Fig. 7a–c
<i>Epigondolella uniformis</i> (16)	Holotype	Orchard 1991: Plate 3, Figs. 1–3
<i>Epigondolella vialovi</i> (17)	Mature growth stage	Balini et al. 2010: Plate 3, Fig. 6a–c
<i>Hayashiella carpathica</i> (25)	Holotype	Mock 1979: Plate 1
<i>Hayashiella tivalica</i> (26)	Holotype	Mazza et al. 2012a: Plate 3, Fig. 4a–c
<i>Metapolygnathus communisti</i> (18)	Holotype	Hayashi (1968) reillustrated by Mazza et al. (2011: Fig. 2B)
<i>Metapolygnathus echinatus</i> (19)	Mature growth stage	Mazza et al. 2012a: Plate 8, Fig. 7a–c
<i>Metapolygnathus linguiformis</i> (20)	Mature growth stage	Balini et al. 2010: Plate 4, Fig. 1
<i>Metapolygnathus mazzai</i> (21)	Holotype	Mazza et al. 2012a: Plate 8, Fig. 12
<i>Metapolygnathus mersinensis</i> (22)	Holotype	Moix et al. 2007: Plate 1, Fig. 14
<i>Metapolygnathus parvus</i> (23)	Holotype	Kozur 1972: Plate 6, Fig. 2
<i>Metapolygnathus praecomunisti</i> (24)	Holotype	Mazza et al. 2011: Fig. 2C
<i>Paragondolella noah</i> (27)	Holotype	Hayashi (1968) reillustrated by Mazza et al. 2011 (Fig. 2A)
<i>Paragondolella oertlii</i> (28)	Holotype	Rigo et al. 2018: Fig. 2
<i>Paragondolella polygnathiformis</i> (29)	Undetermined growth stage	Rigo et al. 2007: Fig. 4.6a–c
<i>Paragondolella praelindae</i> (30)	Submature growth stage	Mazza et al. 2012a: Plate 7 Fig. 13a–c.

considered. Finally, these axes were illustrated in terms of morphological variation to better visualize covariations between morphological traits. Statistical tests were performed using the *ade4* (Dray et al. 2007) library available in R software.

A permutational multivariate analysis of variance (PERMANOVA) (Anderson 2001) was performed on the STATIS compromise scores using PAST v. 3.16 (Hammer et al. 2001) to test the significance of (1) the shape differences between sinistral and dextral-mirrored elements and (2) the intergeneric morphological differences. PERMANOVA may be critically sensitive to heterogeneity of variance between groups (Anderson and Walsh 2013; Anderson 2017). As the studied groups were balanced, we avoided this problem. To assess whether the slopes of reduced major axes (RMA) of each species calculated in the STATIS

compromise were significantly different, we used the χ^2 test for multiple comparison of RMA slopes available in PAST. Correlation between shape variables was tested in R using the Spearman's correlation coefficient in order to account for nonnormality of these variables, and graphic representations were produced using the R package 'ggplot2' (Wickham 2016). In all analyses, $\alpha = 5\%$.

The data sets analyzed in this study and the lines of code we used in R are available as Supplementary Material.

Results

Main Patterns of Shape Variation.—The quantification of the morphological characters of the elements was done on the three standard views. There was no significant morphological difference between dextral-mirrored and

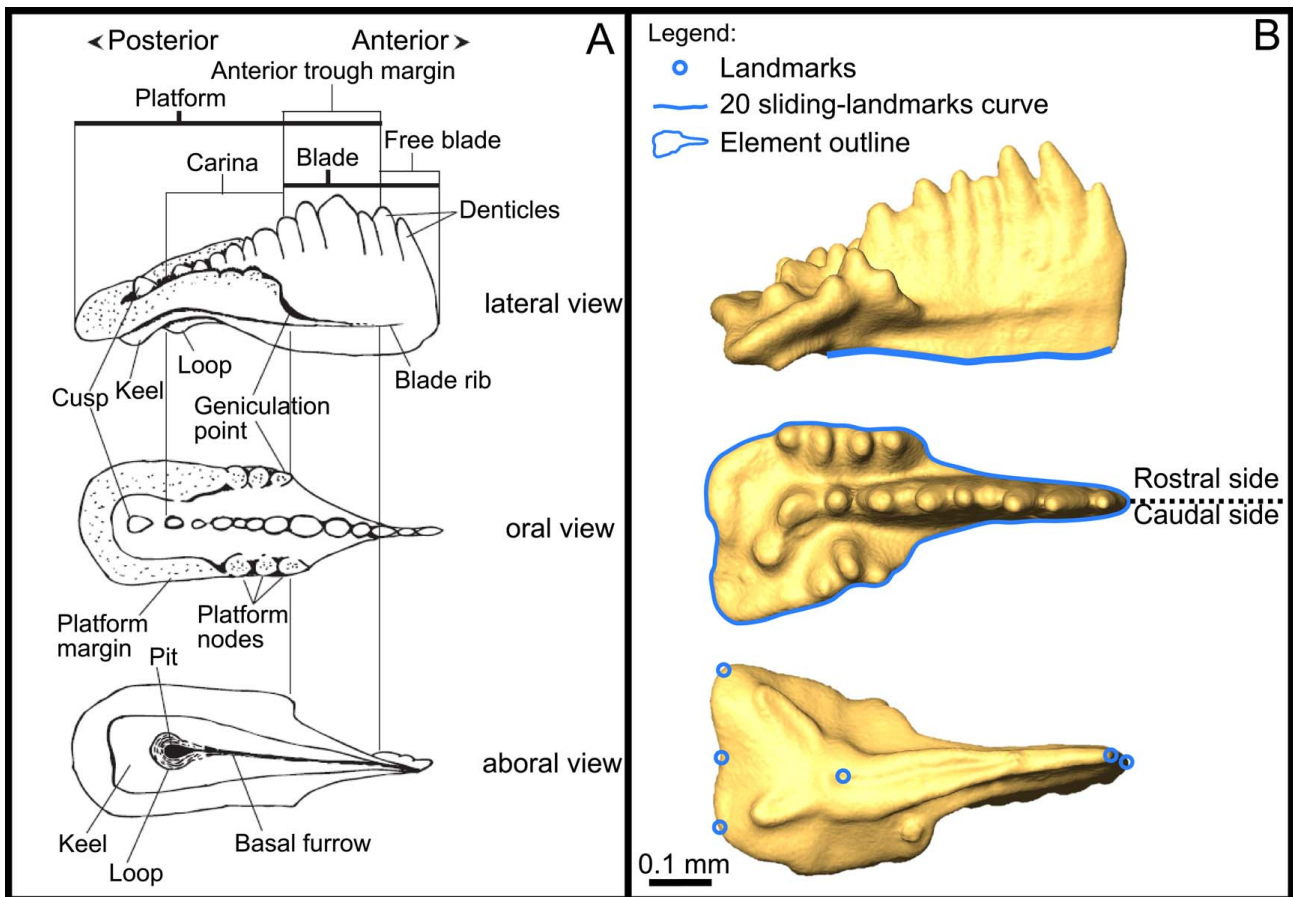


FIGURE 2. A, Definition of P_1 morphological terms from Mazza et al. (2012b); B, location of the landmarks used, sliding-landmarks curve, and outline. The illustrated specimen belongs to *Epigondolella rigoi*.

sinistral elements for each quantified character (PERMANOVA performed on aligned and harmonic coordinates, $p > 0.2$). Hence, the dextral-mirrored images were included in the data set and treated equally as sinistral elements in further analyses.

The three data sets were analyzed independently using a PCA. For each data set, only the most significant PCA axes explaining together at least 80% of the cumulated variance were considered.

The analysis of the lower margin in lateral view (Fig. 3A) returns two principal axes of morphological variation:

- The first axis (69.6% of explained variability, “lower margin bending”) corresponds to the flexure of the lower margin, ranging from semi-elliptic (upward bending) to “wavy” (associated with a stronger downward bending of the posterior end) for the most extreme morphotypes;

- The second axis (14.0%, “lower margin posterior dip”) highlights posterior modifications of the lower margin, with a more or less conspicuous dip of the posteriormost end of the anterior process.

The analysis of the element outline in oral view highlights four main axes of variation (Fig. 3B):

- The first axis (38.8% of explained variability, “platform lateral expansion”) corresponds to variation in the overall width of the platform.
- The second axis (23.8%, “squarobovaticity”) corresponds to variation between elements with a short (about half the length of the element), subsquared platform and elements with an obovate platform (ovate shape with tapering toward the anterior end).
- The third axis (11.0%, “cuneospatulaticity”) illustrates the variation between long wedge-

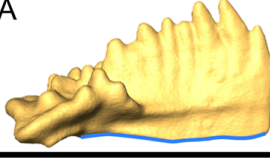
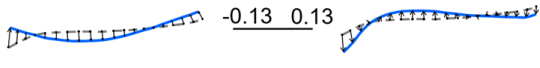
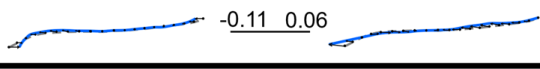
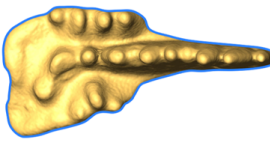
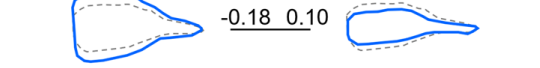
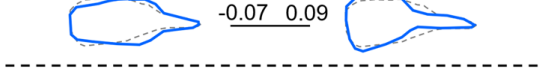
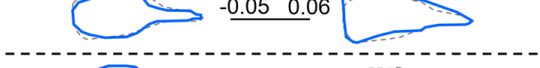
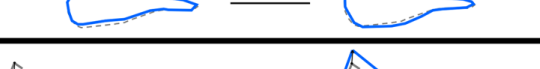
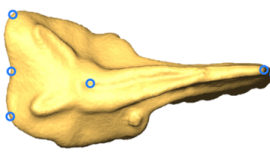
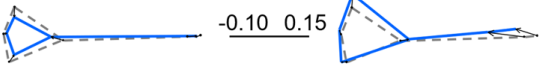
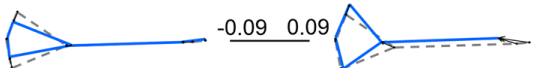
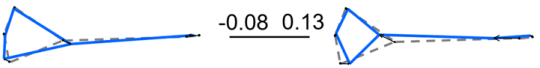
Views	PCA axes	Shape variation	Name of shape indicator
	Axis 1 (69.6%)	 -0.13 0.13	Lower margin bending
	Axis 2 (14.0%)	 -0.11 0.06	Lower margin posterior dip
	Axis 1 (38.8%)	 -0.18 0.10	Platform lateral expansion
	Axis 2 (23.8%)	 -0.07 0.09	Squarobovaticity
	Axis 3 (11.0%)	 -0.05 0.06	Cuneospatulaticity
	Axis 4 (6.6%)	 -0.05 0.05	Element longitudinal bending
	Axis 1 (42.1%)	 -0.10 0.15	Posterior extension
	Axis 2 (22.8%)	 -0.09 0.09	Posterior width
	Axis 3 (20.6%)	 -0.08 0.13	Posterior asymmetry

FIGURE 3. Selected principal components (shape variables) for each view. A, lateral view, lower margin curve; B, oral view, outline analysis; and C, aboral view, set of six landmarks. For each PCA, the percentage of explained variance is given; the extreme morphotypes are represented in solid line (associated with the corresponding score along the axis) as superimposed on the consensus shape represented in dashed line (average shape of the assemblage). The illustrated specimen belongs to *Epigondolella rigoi*.

shaped (“cuneate”) elements and spoon-shaped (“spatulate”) elements with a relatively short and elliptical platform.

- The fourth axis (6.6%, “element longitudinal bending”) corresponds to the overall bending and asymmetry of the element.

In aboral view, the variation of the relative position of the pit can be summarized by three principal components (Fig. 3C):

- The first axis (42.1% of explained variability, “posterior extension”) corresponds to a variation of the dimensions of the posterior end of the elements relative to the entire element: the triangle defined by the two posteriormost corners and the pit remains subequilateral or isosceles, while the size of this triangle varies between one-third and two-fifths of the element length.
- The second axis (22.8%, “posterior width”) corresponds to variation in the relative length

of the posterior part, which gets slightly shorter when the platform gets relatively wider. In other words, it corresponds to lateral expansion of the posterior end of the platform.

- The third axis (20.6%, “posterior asymmetry”) illustrates variation in asymmetry of the posterior part of the element: the more asymmetrical, the shorter the posterior end; additionally, the wider side gets deflected anteriorly.

Combined Analysis of the Three Geometric Morphometrics Data Sets.—To explore the overall shape variation within this assemblage and to assess the weight of each shape descriptor on the global variation, we used the STATIS method. For each view, we projected the principal components described earlier onto the three-table STATIS compromise (built on the three sets of morphometric variables), and then analyzed their relative importance using a correlation circle (Fig. 4B). The specimens of

Hayashiella, *Carnepigondolella*, and their supposed descendants (representatives of *Metapolygnathus* and *Epigondolella*) group in two significantly distinct clusters in the STATIS compromise (PERMANOVA, $p < 0.001$). The axis along which these two groups are most discriminated makes an angle of about 45° with the first STATIS component (Fig. 4A, C1 = 33.5% of the total variance). Furthermore, the main axes of intraspecific variation (i.e., the major axes of each specific ellipse) do not differ significantly from one another (overall χ^2 test for RMA slope comparison: $\chi^2 = 6.0$, $p = 0.24$), highlighting a pattern of intraspecific variation shared by all analyzed taxa (Fig. 4A). This common axis of intraspecific variation appears subperpendicular to the axis separating the two main clusters.

Using the correlation circles we can interpret these observations in terms of biologically meaningful, morphological parameters (Fig. 4B). On one hand, the parameters that most align with the axis separating the “Carnian” ancestors from their presumed “Norian” descendants are the lower margin bending, the squarobovaticity, and the posterior asymmetry. Note also that the nonaligned posterior extension has a greater contribution than the posterior asymmetry in the morphological transformation associated with this intergeneric axis (the projection of the corresponding arrow on the separation axis is larger than the one for posterior asymmetry). In other words, the transition from *Hayashiella* and *Carnepigondolella* to *Epigondolella* and *Metapolygnathus* in this data set corresponds, in P₁ elements, to a more upward-bent lower margin, a shorter and squarer platform, and a relatively larger posterior part.

On the other hand, the platform lateral extension and the posterior width are the parameters most aligned with the common axis of intraspecific variation. This suggests that, within a given species, elements tend to show varying degrees of platform lateral expansion associated with modifications of the relative width of the posterior part: the larger the lateral expansion of the platform, the larger the posterior part (in overall size relative to element length) but the narrower the posterior part, and the more elliptic the element.

As is implicit from the patterns of variation described, most parameters are covarying to some degree. In particular, the lower margin bending, squarobovaticity, and posterior extension are significantly pairwise correlated (Spearman’s correlation test, $0.57 < |\rho| < 0.74$, $p < 0.001$; Fig. 5). Likewise, platform lateral extension and posterior width are negatively correlated (Spearman’s correlation test, $\rho = -0.52$, $p < 0.001$).

As with the STATIS compromise (Fig. 4A), species are hardly distinguished from one another based on a single pair of characters: the spread of the intraspecific variation is usually much greater than the distance between the means of two given species. The distinction between the Carnian and Norian forms analyzed in this study is driven by the lower margin bending. In this data set, carnepigondolellid and hayashiellid forms tend to have a relatively longer platform that is obovate in oral view, a posteriorly located pit, and a wavy lower margin. Epigondolellid forms tend to have a relatively short platform and a large posterior end (squared), a centrally located pit, and a semi-elliptic lower margin. *Metapolygnathus* appears as intermediate between them for the considered descriptors.

To best represent the overall morphological variation of *Paragondolella*, *Carnepigondolella*, *Metapolygnathus*, *Hayashiella*, and *Epigondolella* at Pizzo Mondello, the holotypes and representatives of 30 conodont species were added to the STATIS analysis (Fig. 4C). The structure of the morphospace was found similar to the one previously described with the seven studied species only. The holotypes of the studied species fall within the range of variation of the samples, except for those of *Hayashiella tivalica*, *E. quadrata*, and *E. uniformis*, which remain close to their species sample variation range. It is unclear whether this shift is due to an orientation bias introduced by using photographs from the literature produced by different authors. *Paragondolella* and *Carnepigondolella* are located in the same area, and they are separated from their supposed descendants, *Epigondolella* and *Metapolygnathus*.

Discussion

This study focused on the analysis of the morphological variation and covariation of a

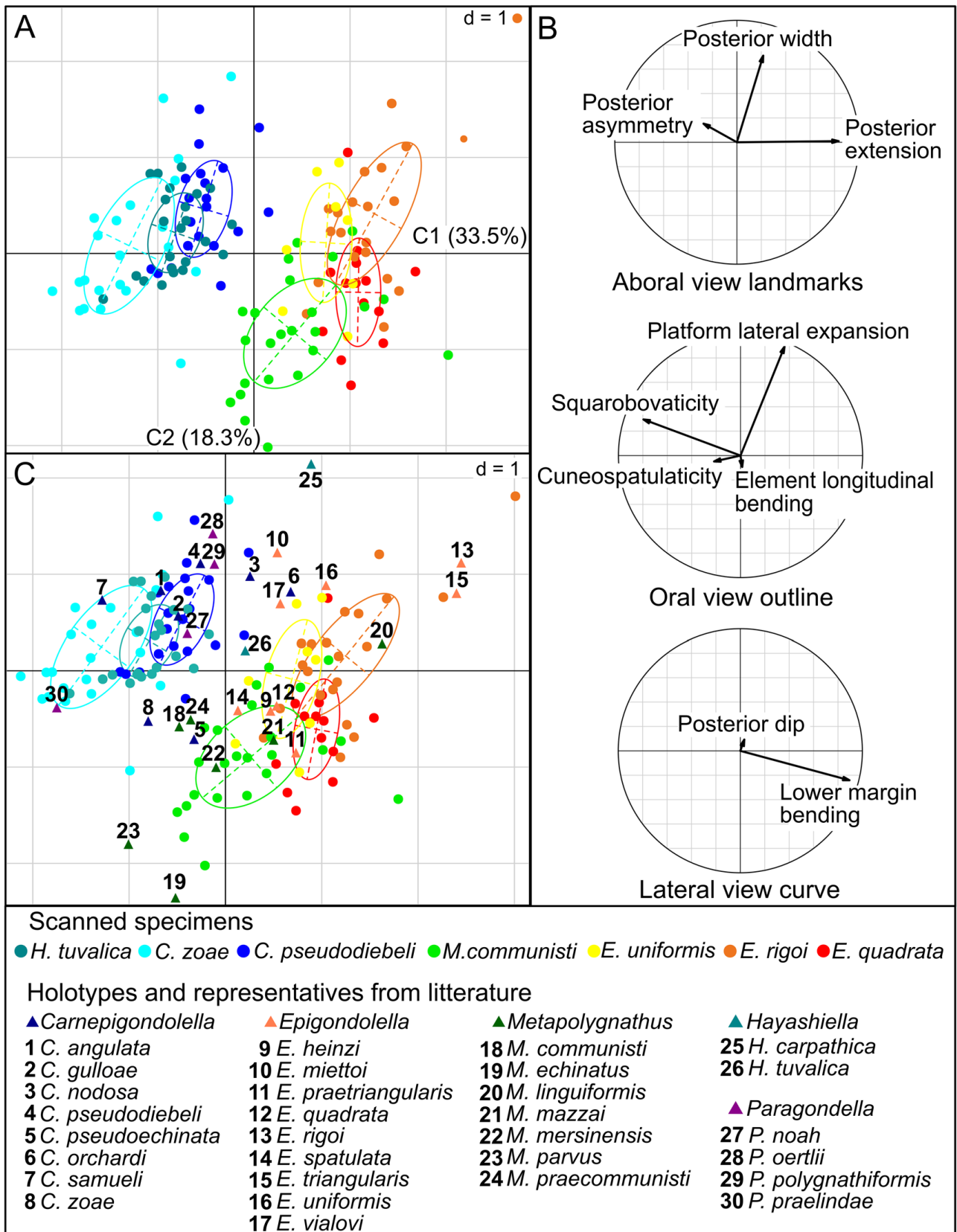
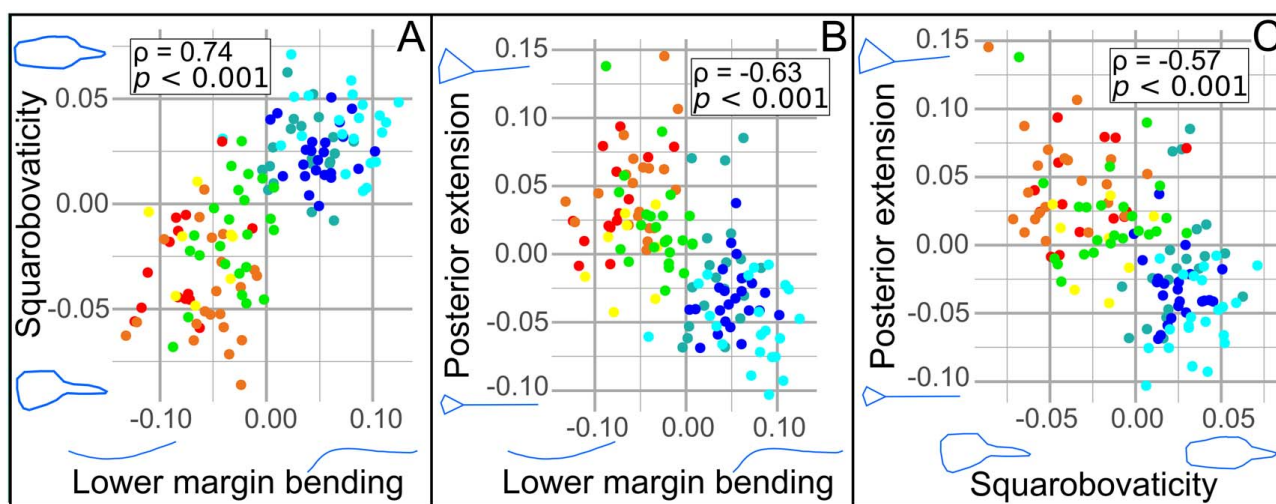


FIGURE 4. A, The first two axes (C1 and C2) of the STATIS compromise showing the best separation of specimens (dots) associated to the three sets of coordinates. Ellipses (63% of the specimens within a given species) identify specimens belonging to a given species (the scale “d” corresponds to the grid size). B, The first two axes of a STATIS compromise correlation circle showing the projections of the principal components of separate PCAs selected in Fig. 3. C, The first two axes of the STATIS compromise with holotypes and representatives of species included in the phylogenetic hypothesis of conodonts from the Pizzo Mondello section. Abbreviations for the legend: *C.*, *Carnepigondolella*; *H.*, *Hayashiella*; *E.*, *Epigondolella*; *M.*, *Metapolygnathus*; *P.*, *Paragondolella*.



Legend

- *Carnepigondolella pseudodiebeli* ● *Metapolygnathus communisti* ● *Epigondolella quadrata*
- *Carnepigondolella zoae* ● *Epigondolella rigoi*
- *Hayashiella tuvalica* ● *Epigondolella uniformis*

FIGURE 5. Correlations between A, Lower margin bending and squarobovaticity; B, lower margin bending and posterior extension; C, squarobovaticity and posterior extension. All correlations were tested by a coefficient of Spearman's correlation (ρ) and a p -value (p). Each species is associated with a single color.

data set of Late Triassic (late Carnian to early Norian) P₁ conodont elements. The STATIS analysis shows that the Carnian basal forms clearly differ from the Norian derived forms. On one hand, the intraspecific and intergeneric morphological variations correspond to two distinct patterns driven by characters that covary at both taxonomic levels (Fig. 6). On the other hand, the different species within each of these groups cannot be distinguished using only the morphological traits considered here.

The Morphological Characters: Different Implications at Different Taxonomic Levels.—Within each genus, the intraspecific variation usually overlaps in the three-table STATIS compromise. This can be due to the fact that the ornamentation of the platform and the morphology of the keel end were not quantified here, as we considered only the characters that are present in all taxa, which is not the case for platform ornamentation and the keel morphology. Nevertheless, this morphological analysis shows that: (1) a few characters are sufficient to group related species and to reveal the morphological transformations that occurred between the basal and the derived groups (i.e., the lower margin bending, the squarobovaticity, and the

posterior extension, Fig. 4A); (2) the same morphological transformations were involved in the evolution of two separate lineages (i.e., parallel evolution between *Carnepigondolella*–*Metapolygnathus* and *Carnepigondolella*–*Epigondolella*; Figs. 4, 5); and (3) the characters driving variation at the intraspecific level (i.e., the posterior width and the platform lateral expansion) differ from those driving morphological variation at the intergeneric level (Fig. 4A,B).

This study highlights for the first time a common pattern of intraspecific variation within a conodont assemblage consisting of closely related taxa. All the available adult specimens that were preserved well enough to conduct the geometric morphometric analysis were considered, thus avoiding any “cherry-picking” bias. Nevertheless, the elements analyzed here represent only a portion of the available material, as the method requires fully preserved conodonts. Because the specimens had been already determined and hence classified into specific bins, the observed consistency of the intraspecific variation may correspond to a generic concept of conodont species variability, even if unlikely.

Global Environmental Disturbance as an Explanation for the Morphological Shift.—The

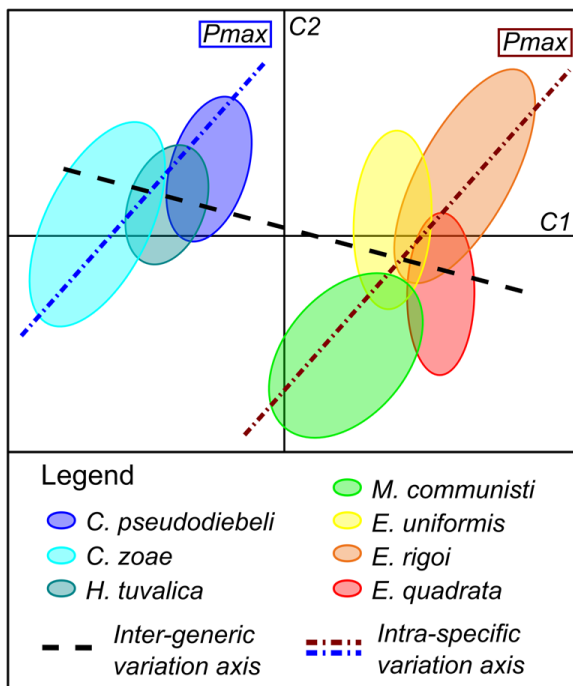


FIGURE 6. Illustration of the inter- vs. intraspecific patterns of variation based on the first two axes (C1 and C2) of the STATIS compromise. The ellipses identify species. *C.*, *Carnepigondolella*; *H.*, *Hayashiella*; *E.*, *Epigondolella*; *M.*, *Metapolygnathus*.

studied data set can also be used to investigate environmental versus developmental drivers of conodont evolution within the analyzed time series by using the theoretical framework of the lines of least evolutionary resistance (Schluter 1996; Renaud et al. 2006; Hunt 2007). According to this theory, species would evolve preferentially along the main axis of intraspecific phenotypic variance (P_{max}). Further, any significant deviation from the P_{max} trajectory can be interpreted as reflecting the influence of nonrandom selective factors such as environmental pressures.

The fact that the main intergeneric axis of phenotypic variance is almost perpendicular to P_{max} in two separate lineages strongly suggests that the evolution of these Norian forms was driven by an external perturbation (Fig. 6). The location within the morphospace of the *Paragondolella* specimens among *Carnepigondolella*–*Hayashiella* specimens is consistent with this hypothesis (Fig. 4).

Note also that the main morphological trends between Carnian and Norian forms are observed independently of taxonomic classifications, because they were also described, with the exception of the lower-margin profile

of the platform, by Orchard (2014), based on similar collections from the Black Bear Ridge section in Canada, and despite a divergent view on taxonomy and phylogeny of these conodonts.

As the Pizzo Mondello section is a GSSP candidate for the definition of the CNB, detailed geochemical and paleontological studies have been already carried out (Mazza et al. 2010, 2012b), and their results can be interpreted in terms of paleoenvironments. The stable carbon isotope record (Mazza et al. 2010) of the Pizzo Mondello section shows a quasi 1‰ positive excursion at the base of the CNB interval (Muttoni et al. 2004: Fig. 3, at 84.5 m; Mazza et al. 2010: Fig. 5, at 82 m). This approximately 1‰ positive shift coincides with the most conspicuous faunal turnover in this section: most of the carnepigondolellids go extinct and specimens of *Metapolygnathus* and *Epigondolella* become abundant (Fig. 7). A similar positive shift of $\delta^{13}\text{C}$ along with a conodont turnover is observed around the CNB at Black Bear Ridge, Canada, on the other side of Pangea. Onoue and coworkers (2016) interpreted this $\delta^{13}\text{C}$ shift as resulting from anoxic conditions. Mazza and coworkers (2010), on the other hand, interpreted the shift in Pizzo Mondello as resulting from an expansion of photosynthetically active organisms. Despite these different interpretations (note that both are not mutually exclusive), paleoenvironmental and faunal changes around CNB were not restricted to Pizzo Mondello and were likely of global extent.

At the global scale, a 1.5‰ increase of the Tethyan subtropics stable oxygen isotope ratio ($\delta^{18}\text{O}_{\text{apatite}}$, measured on conodont elements) from the late Tuvalian (late Carnian) to the early Lacin (early Norian) was demonstrated by several authors (Rigo and Joachimski 2010; Rigo et al. 2012; Trotter et al. 2015), implying a decrease of 6°C in seawater temperature. This cooling followed the Wrangellian volcanism and the Carnian pluvial episode and marked a return to an arid climate. It coincided with low pCO_2 values (Fletcher et al. 2008) and a major faunal turnover at several trophic levels: replacement of almost all coral species (Stanley 1988) and emergence and radiation of new phytoplankton (dinoflagellates and

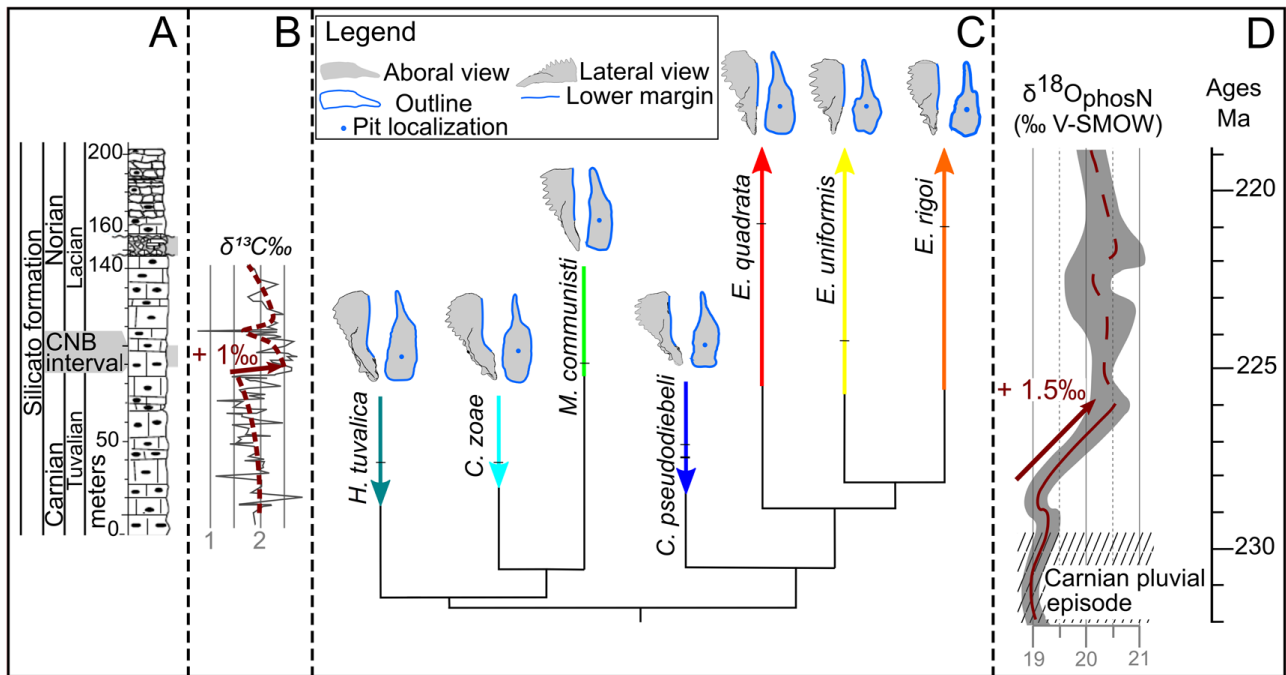


FIGURE 7. Synthetic illustration including sedimentologic, geochemical, stratigraphic, and morphological data of the Pizzo Mondello section and at global scale. A, Log including the Carnian/Norian boundary (CNB) interval, and a part of the upper Carnian and lower Norian (after Mazza et al. [2012a]). B, $\delta^{13}\text{C}$ isotopic data obtained from carbonate bulk sample, including the 1‰ shift occurring just before the CNB interval (Mazza et al. 2010). The dashed line and the arrow highlight the shift (image modified after Mazza et al. [2010]). C, Global stratigraphically calibrated cladogram reduced to the seven studied species (modified after Rigo et al. [2018]). The stratigraphic range, location of the samples used in this study, and specimen consensus are represented for each species. D, Global conodont-based $\delta^{18}\text{O}$ isotopic curve showing the 1.5‰ positive shift (modified after Trotter et al. [2015]). Absolute timing calibration was based on Kent et al. (2017).

coccoliths) lineages (Payne and Van de Schootbrugge 2007) and marine and terrestrial vertebrates, including dinosaurs, pterosaurs, turtles, crocodylians, and mammals (Benton et al. 2014). This suggests a major shift in available food resources, and conodonts were likely affected by this shift. The morphological evolution of their P_1 elements may thus reflect adaptations to new diets.

A Link between Shape and Function.—Hitherto, no functional model has been available for the studied lineages. Yet, Martínez-Pérez et al. (2014a, b, 2016) analyzed different platform-bearing P_1 elements using 3D models, microwear observations, and finite element analysis. For instance, they suggested that the evolution of the platform in *Polygnathus* may reflect an increased accommodation to biomechanical stress—in other words, a stronger bite (Martínez-Pérez et al. 2016). Extrapolating these studies to the present material, it seems likely that the P_1 elements of *Carnepigondolella* and *Metapolygnathus–Epigondolella*, respectively, correspond to different occlusal

mechanics (see next paragraph), a possible topic for future research.

As suggested previously (Mosher 1968; Mazza et al. 2012a), the transition from Carnian to Norian forms involved modifications of the lower-margin profile of the platform (captured in the lower margin bending principal component), a shortening of the platform relative to the entire element (see brevicuneoellipticity and posterior extension principal components), and a shifting of the pit (i.e., a relative enlargement of the posterior part of the element; see posterior extension) (Figs. 7, 8). Moreover, even if it was not quantified here, the ornamentation of the platform became more complex, showing a development from nodes restricted to the middle and anterior parts of the platform (Carnian) to nodes or denticles all over the platform (Norian) (Mazza et al. 2012a). The combination of a wavy baseline and a poor platform ornamentation (*Carnepigondolella* group) may reflect a rotational movement of the P_1 elements, whereby occlusion starts in the anterior part of the element with a

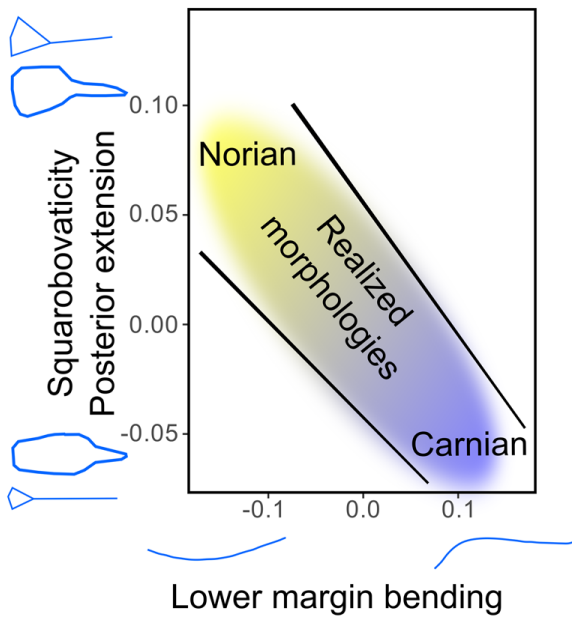


FIGURE 8. Illustration of the constrained morphologies of the conodont elements through the Carnian/Norian interval.

blade-to-blade contact (which may have functioned as an occlusional guide or as a cutting device) and ends in the posterior part with a platform-to-platform contact that was likely used for crushing food items. On the other hand, the combination of a semi-elliptic baseline and a strong platform ornamentation (*Epi-gondolella* species) suggests a translational movement of the P_1 elements toward one another and a direct occlusion between the sharp platforms that may have been used for perforation and ripping of the food items.

The Developmental Mechanisms under the Evolutionary Shift.—The fact that the very same evolutionary path was followed in two presumably distinct lineages in the Pizzo Mondello section suggests that the morphologies of these two lineages were constrained in a similar way, and possibly by the same drivers. Beyond the patterns of intraspecific and intergeneric variation, the correlations we demonstrated between, on one hand, the lower margin bending, squarobovaticity, and posterior extension (and, implicitly, platform ornamentation), and on the other hand, the posterior width and platform lateral expansion also emphasize the existence of “restricted” areas in the morphospace for which no realized morphology is observed (Fig. 8; see also Fig. 5). As far as P_1 conodont

elements are concerned, this suggests that general laws of covariation exist that apply not only within species, but also at higher taxonomic levels. These laws may be the consequence of some developmental and/or functional constraints. For instance, the association of a wavy baseline and a large posterior platform (and/or a highly ornamented platform) is never observed in this assemblage. While different observed morphological associations may reflect different feeding mechanisms (see “A Link between Shape and Function”), nonobserved associations may correspond to morphologies that are either developmentally “impossible” or functionally “nonviable,” because they could prevent proper occlusion and hence proper feeding.

The effect of environmental changes has often been at the core of evolutionary studies in deep time, whereas the developmental aspects of the considered organisms have often been neglected. Inferring developmental constraints from the fossil record is not an easy task, but as we have shown, it is not an impossible one (see also Ciampaglio 2002; Moulton et al. 2012; Urdy et al. 2013; Erlich et al. 2016). Paleo-eco-evo-devo studies are thus feasible and are likely, in the near future, to tremendously enhance our understanding of the evolutionary processes that shaped and are shaping life.

Conclusion

A parallel evolutionary path between two lineages, highlighted by a common pattern of intraspecific and intergeneric variation, suggests the existence of generic laws of morphological trait covariation in conodont elements. The transition between Carnian forms and their presumed Norian descendants corresponds to an axis in the morphospace that is very different from the axis of intraspecific variation affecting all pre- and post-CNB species, suggesting that the intergeneric evolution of these elements did not follow the expected evolutionary path of least resistance. This may reflect the consequences of an environmental disturbance, as emphasized by the carbon and oxygen stable isotope records during that particular interval, and/or its ecological

implications for conodonts, such as a possible diet change. This would have constituted a selective pressure on the shapes of conodont elements. The present study is a first step toward a general quantification and better understanding of the patterns of variation and covariation in euconodonts, and hence a better interpretation of their morphological evolution. Thanks to their ~300-Myr-long, widespread abundance in marine strata, conodont elements appear to be a very useful model to study evolutionary processes in deep time.

Acknowledgments

We thank Mathilde Bouchet (ENS Lyon, SFR Biosciences) for her invaluable help with the microtomography and Gilles Escarguel (Université Lyon 1) for his advice on statistics. Gilles Escarguel is also thanked for having discussed several drafts of this article. Finally, we thank Emilia Jarochowska, Carlos Martínez-Pérez, and an anonymous reviewer who corrected the draft and helped to improve this article. This research is supported by a French ANR @RAction grant to N.G. (ACHN project EvoDevOdonto).

Literature Cited

- Anderson, M. J. 2001. A new method for non-parametric multivariate analysis of variance. *Austral Ecology* 26:32–46.
- . 2017. Permutational multivariate analysis of variance (PERMANOVA). Wiley statsRef: statistics reference online. doi: 10.1002/9781118445112.stat07841.
- Anderson, M. J., and D. C. Walsh. 2013. PERMANOVA, ANOSIM, and the Mantel test in the face of heterogeneous dispersions: what null hypothesis are you testing? *Ecological Monographs* 83:557–574.
- Balini, M., A. Bertinelli, P. Di Stefano, C. Guaiumi, M. Levera, M. Mazza, G. Muttoni, A. Nicora, N. Preto, and M. Rigo. 2010. The late Carnian–Rhaetian succession at Pizzo Mondello (Sicani Mountains). *Albertiana* 39:36–57.
- Barnett, S. G. 1972. The evolution of *Spathognathodus remscheidensis* in New York, New Jersey, Nevada, and Czechoslovakia. *Journal of Paleontology* 46:900–917.
- Benton, M. J., J. Forth, and M. C. Langer. 2014. Models for the rise of the dinosaurs. *Current Biology* 24:R87–R95.
- Blanc, L., D. Chessel, and S. Dolédec. 1998. Etude de la stabilité temporelle des structures spatiales par analyses d'une série de tableaux de relevés faunistiques totalement appariés. *Bulletin Français de la Pêche et de la Pisciculture* 348:1–21.
- Bonhomme, V., S. Picq, C. Gaucherel, J. Claude. 2014. Momocs: outline analysis using R. *Journal of Statistical Software* 56:1–24.
- Chen, J., T. W. Beatty, C. M. Henderson, and H. Rowe. 2009. Conodont biostratigraphy across the Permian–Triassic boundary at the Dawen section, Great Bank of Guizhou, Guizhou Province, South China: implications for the Late Permian extinction and correlation with Meishan. *Journal of Asian Earth Sciences* 36:442–458.
- Chen, Y., T. A. Neubauer, L. Krystyn, and S. Richo. 2016. Allometry in Anisian (Middle Triassic) segminiplanate conodonts and its implications for conodont taxonomy. *Palaeontology* 59:725–741.
- Ciampaglio, C. N. 2002. Determining the role that ecological and developmental constraints play in controlling disparity: examples from the crinoid and blastozoan fossil record. *Evolution and Development* 4:170–188.
- Condamine, F. L., J. Rolland, and H. Morlon. 2013. Macroevolutionary perspectives to environmental change. *Ecology Letters* 16:72–85.
- Croll, V. M., R. J. Aldridge, and P. K. Harvey. 1982. Computer applications in conodont taxonomy: characterization of blade elements. Miscellaneous paper. Geological Society of London, Computer Applications in Geology I & II 14:237–246.
- Donoghue, P. C. 1998. Growth and patterning in the conodont skeleton. *Philosophical Transactions of the Royal Society of London B* 353:633–666.
- Donoghue, P. C., and M. A. Purnell. 1999. Growth, function, and the conodont fossil record. *Geology* 27:251–254.
- Donoghue, P. C., P. L. Forey, and R. J. Aldridge. 2000. Conodont affinity and chordate phylogeny. *Biological Reviews* 75:191–251.
- Dray, S., A. B. Dufour, and D. Chessel. 2007. The ade4 package-II: two-table and K-table methods. *R News* 7:47–52.
- Epstein, A. G., J. B. Epstein, and L. D. Harris. 1977. Conodont color alteration: an index to organic metamorphism. Geological Survey Professional Paper 995. U.S. Government Printing Office, Washington, D.C.
- Erlich, A., D. E. Moulton, A. Goriely, and R. Chirat. 2016. Morphomechanics and developmental constraints in the evolution of ammonites shell form. *Journal of Experimental Zoology B* 326:437–450.
- Erwin, D. H. 2017. Developmental push or environmental pull? The causes of macroevolutionary dynamics. *History and Philosophy of the Life Sciences* 39:36.
- Fletcher, B. J., S. J. Brentnall, C. W. Anderson, R. A. Berner, and D. J. Beerling. 2008. Atmospheric carbon dioxide linked with Mesozoic and early Cenozoic climate change. *Nature Geoscience* 1:43.
- Girard, C., and S. Renaud. 2007. Quantitative conodont-based approaches for correlation of the Late Devonian Kellwasser anoxic events. *Palaeogeography, Palaeoclimatology, Palaeoecology* 250:114–125.
- . 2008. Disentangling allometry and response to Kellwasser anoxic events in the Late Devonian conodont genus *Ancyrodella*. *Lethaia* 41:383–394.
- . 2011. The species concept in a long-extinct fossil group, the conodonts. *Comptes Rendus Palevol* 10:107–115.
- Girard, C., S. Renaud, and D. Korn. 2004a. Step-wise morphological trends in fluctuating environments: evidence in the Late Devonian conodont genus *Palmatolepis*. *Geobios* 37:404–415.
- Girard, C., S. Renaud, and A. Sérayet. 2004b. Morphological variation of *Palmatolepis* Devonian conodonts: species versus genus. *Comptes Rendus Palevol* 3:1–8.
- Goudemand, N., M. J. Orchard, S. Urdy, H. Bucher, and P. Tafforeau. 2011. Synchrotron-aided reconstruction of the conodont feeding apparatus and implications for the mouth of the first vertebrates. *Proceedings of the National Academy of Sciences USA* 108:8720–8724.
- Hallam, A. 1996. Major bio-events in the Triassic and Jurassic. Pp. 265–283 in O. H. Walliser, ed. *Global events and event stratigraphy in the Phanerozoic*. Springer, Berlin.
- Hammer, Ø., D. A. T. Harper, and P. D. Ryan. 2001. Paleontological statistics software: package for education and data analysis. *Palaeontologia Electronica* 4:9.
- Hayashi, S. 1968. The Permian conodonts in chert of the Adoyama Formation, Ashio mountains, central Japan. *Earth Science* 22:63–77.

- Hunt, G. 2007. Evolutionary divergence in directions of high phenotypic variance in the ostracode genus *Poseidonamicus*. *Evolution* 61:1560–1576.
- Huxley, J. 1942. *Evolution: the modern synthesis*. George Allen and Unwin, London.
- Jablonski, D. 2017. Approaches to macroevolution: 1. General concepts and origin of variation. *Evolutionary Biology* 44:427–450.
- Joachimski, M. M., R. D. Pancost, K. H. Freeman, C. Ostertag-Henning, and W. Buggisch. 2002. Carbon isotope geochemistry of the Frasnian–Famennian transition. *Palaeogeography, Palaeoclimatology, Palaeoecology* 181:91–109.
- Joachimski, M. M., P. H. von Bitter, and W. Buggisch. 2006. Constraints on Pennsylvanian glacioeustatic sea-level changes using oxygen isotopes of conodont apatite. *Geology* 34:277–280.
- Jones, D. 2009. Directional evolution in the conodont *Pterospathodus*. *Paleobiology* 35:413–431.
- Jones, D., M. A. Purnell, and P. H. von Bitter. 2009. Morphological criteria for recognising homology in isolated skeletal elements: comparison of traditional and morphometric approaches in conodonts. *Palaeontology* 52:1243–1256.
- Kent, D. V., P. E. Olsen, and G. Muttoni. 2017. Astrochronostratigraphic polarity time scale (APTS) for the Late Triassic and Early Jurassic from continental sediments and correlation with standard marine stages. *Earth-Science Reviews* 166:153–180.
- Klapper, G., and C. T. Foster, Jr. 1993. Shape analysis of Frasnian species of the Late Devonian conodont genus *Palmatolepis*. *Paleontological Society Memoir* 32. *Journal of Paleontology* 67:1–35.
- Kozur, H. 1972. Die Conodontengattung *Metapolygnathus* (Hayashi, 1968) und ihr stratigraphischer Wert (Conodont genus *Metapolygnathus* (Hayashi, 1968) and their stratigraphic values). Institut für Geologie und Paläontologie, Münster, Germany. [In German.]
- Kuhl, F. P., and C. R. Giardina. 1982. Elliptic Fourier features of a closed contour. *Computer Graphics and Image Processing* 18:236–258.
- Lavit, C., Y. Escoufier, R. Sabatier, and P. Traissac. 1994. The ACT (STATIS method). *Computational Statistics & Data Analysis* 18:97–119.
- Levins, R., and R. C. Lewontin. 1985. *The dialectical biologist*. Harvard University Press, Cambridge.
- Martínez-Pérez, C., P. Plasencia, D. Jones, T. Kolar-Jurkovšek, J. Sha, H. Botella, and P. C. Donoghue. 2014a. There is no general model for occlusal kinematics in conodonts. *Lethaia* 47:547–555.
- Martínez-Pérez, C., E. J. Rayfield, M. A. Purnell, and P. C. Donoghue. 2014b. Finite element, occlusal, microwear and microstructural analyses indicate that conodont microstructure is adapted to dental function. *Palaeontology* 57:1059–1066.
- Martínez-Pérez, C., M. A. Purnell, E. Rayfield, and P. C. J. Donoghue. 2016. Shedding light into the function of the earliest vertebrate skeleton. EGU General Assembly Conference Abstracts 18:17108.
- Mayr, E. 1982. Speciation and macroevolution. *Evolution* 36:1119–1132.
- Mazza, M., and C. Martínez-Pérez. 2015. Unravelling conodont (Conodonta) ontogenetic processes in the Late Triassic through growth series reconstructions and X-ray microtomography. *Bollettino della Società Paleontologica Italiana* 54:161–186.
- . 2016. Evolutionary convergence in conodonts revealed by synchrotron-based tomographic microscopy. *Palaeontologia Electronica* 19:1–11.
- Mazza, M., S. Furin, C. Spötl, and M. Rigo. 2010. Generic turnovers of Carnian/Norian conodonts: climatic control or competition? *Palaeogeography, Palaeoclimatology, Palaeoecology* 290:120–137.
- Mazza, M., M. Rigo, and A. Nicora. 2011. A new *Metapolygnathus* platform conodont species and its implications for Upper Carnian global correlations. *Acta Palaeontologica Polonica* 56:121–131.
- Mazza, M., A. Cau, and M. Rigo. 2012a. Application of numerical cladistic analyses to the Carnian–Norian conodonts: a new approach for phylogenetic interpretations. *Journal of Systematic Palaeontology* 10:401–422.
- Mazza, M., M. Rigo, and M. Gullo. 2012b. Taxonomy and biostratigraphic record of the Upper Triassic conodonts of the Pizzo Mondello section (western Sicily, Italy), GSSP candidate for the base of the Norian. *Rivista Italiana di Paleontologia e Stratigrafia* 118:85–130.
- Mazza, M., A. Nicora, and M. Rigo. 2018. *Metapolygnathus parvus* Kozur, 1972 (Conodonta): a potential primary marker for the Norian GSSP (Upper Triassic). *Bollettino della Società Paleontologica Italiana* 57:81–101.
- Mock, R. 1979. *Gondolella carpathica* n. sp., eine wichtige tuvalische Conodontenart. *Geologisch-Paläontologische Mitteilungen Innsbruck* 9:171–174.
- Moix, P., H. W. Kozur, G. M. Stampfli, and H. Mostler. 2007. New paleontological, biostratigraphical and paleogeographic results from the Triassic of the Mersin Mélange, SE Turkey. The global Triassic. *New Mexico Museum of Natural History Science Bulletin* 41:282–311.
- Mosher, L. C. 1968. Evolution of Triassic platform conodonts. *Journal of Paleontology* 42:947–954.
- Moulton, D. E., A. Goriely, and R. Chirat. 2012. Mechanical growth and morphogenesis of seashells. *Journal of Theoretical Biology* 311:69–79.
- Murdock, D. J., I. J. Sansom, and P. C. Donoghue. 2013. Cutting the first “teeth”: a new approach to functional analysis of conodont elements. *Proceedings of the Royal Society of London B* 280:20131524.
- Murphy, M. A., and M. K. Cebecioglu. 1984. The *Icriodus steinachsenis* and *I. claudiae* lineages (Devonian conodonts). *Journal of Paleontology* 58:1399–1411.
- Murphy, M. A., and K. B. Springer. 1989. Morphometric study of the platform elements of *Amydrotaxis praejohnsoni* n. sp. (Lower Devonian, Conodonts, Nevada). *Journal of Paleontology* 63:349–355.
- Muttoni, G., D. V. Kent, P. E. Olsen, P. Di Stefano, W. Lowrie, S. M. Bernasconi, and F. M. Hernández. 2004. Tethyan magnetostratigraphy from Pizzo Mondello (Sicily) and correlation to the Late Triassic Newark astrochronological polarity time scale. *Geological Society of America Bulletin* 116:1043–1058.
- Nicora, A., M. Balini, A. Bellanca, A. Bertinelli, S. A. Bowring, P. Di Stefano, P. Dumitrica, et al. 2007. The Carnian/Norian boundary interval at Pizzo Mondello (Sicani Mountains, Sicily) and its bearing for the definition of the GSSP of the Norian Stage. *Albertiana* 36:102–129.
- Noyan, Ö. F., and H. W. Kozur. 2007. Revision of the late Carnian–early Norian conodonts from the Stefanion section (Argolis, Greece) and their palaeobiogeographic implications. *Neues Jahrbuch für Geologie und Paläontologie-Abhandlungen* 245:159–178.
- Onoue, T., J.-P. Zonneveld, M. J. Orchard, M. Yamashita, K. Yamashita, H. Sato, and S. Kusaka. 2016. Paleoenvironmental changes across the Carnian/Norian boundary in the Black Bear Ridge section, British Columbia, Canada. *Palaeogeography, Palaeoclimatology, Palaeoecology* 441:721–733.
- Orchard, M. J. 1991. Upper Triassic conodont biochronology and new index species from the Canadian Cordillera. *Bulletin of the Geological Survey of Canada* 417:299–335.
- . 2013. Five new genera of conodonts from the Carnian–Norian boundary beds of Black Bear Ridge, northeast British Columbia, Canada. The Triassic system. *New Mexico Museum of Natural History and Science Bulletin* 61:445–457.
- Orchard, M. J. 2014. Conodonts from the Carnian–Norian boundary (Upper Triassic) of Black Bear Ridge, Northeastern British Columbia. *New Mexico Museum of Natural History and Science* 64:1–139.
- Pálffy, J., A. Demény, J. Haas, E. S. Carter, Á. Görög, D. Halász, A. Oravecz-Scheffer, M. Hetényi, E. Márton, and M. J. Orchard.

2007. Triassic–Jurassic boundary events inferred from integrated stratigraphy of the Csövár section, Hungary. *Palaeogeography, Palaeoclimatology, Palaeoecology* 244:11–33.
- Payne, J. L., and B. Van de Schootbrugge. 2007. Life in Triassic oceans: links between planktonic and benthic recovery and radiation. Pp. 165–189 *in* Evolution of primary producers in the sea. Elsevier, San Diego, Calif.
- Purnell, M. A. 1994. Skeletal ontogeny and feeding mechanisms in conodonts. *Lethaia* 27:129–138.
- Purnell, M. A., P. C. Donoghue, and R. J. Aldridge. 2000. Orientation and anatomical notation in conodonts. *Journal of Paleontology* 74:113–122.
- R Core Team. 2018. R: a language and environment for statistical computing. R Foundation for Statistical Computing, Vienna, Austria.
- Renaud, S., and C. Girard. 1999. Strategies of survival during extreme environmental perturbations: evolution of conodonts in response to the Kellwasser crisis (Upper Devonian). *Palaeogeography, Palaeoclimatology, Palaeoecology* 146:19–32.
- Renaud, S., J.-C. Auffray, and J. Michaux. 2006. Conserved phenotypic variation patterns, evolution along lines of least resistance, and departure due to selection in fossil rodents. *Evolution* 60:1701–1717.
- Rigo, M., and M. M. Joachimski. 2010. Palaeoecology of Late Triassic conodonts: constraints from oxygen isotopes in biogenic apatite. *Acta Palaeontologica Polonica* 55:471–479.
- Rigo, M., N. Preto, G. Roghi, F. Tateo, and P. Mietto. 2007. A rise in the carbonate compensation depth of western Tethys in the Carnian (Late Triassic): deep-water evidence for the Carnian Pluvial Event. *Palaeogeography, Palaeoclimatology, Palaeoecology* 246:188–205.
- Rigo, M., J. A. Trotter, N. Preto, and I. S. Williams. 2012. Oxygen isotopic evidence for Late Triassic monsoonal upwelling in the northwestern Tethys. *Geology* 40:515–518.
- Rigo, M., M. Mazza, V. Karádi, and A. Nicora. 2018. New Upper Triassic conodont biozonation of the Tethyan realm. Pp. 189–235 *in* L. Tanner, ed. *The Late Triassic world*. Springer, Cham.
- Ritter, S. M. 1989. Morphometric patterns in Middle Triassic *Neogondolella momburgensis* (Conodontia), Fossil Hill, Nevada. *Journal of Paleontology* 63:233–245.
- Robert, P., and Y. Escoufier. 1976. A unifying tool for linear multivariate statistical methods: the RV-coefficient. *Applied Statistics*:257–265.
- Roghi, G., P. Mirro, and F. M. Dalla Vecchia. 1995. Contribution to the conodont biostratigraphy of the Dolomia di Forni (Upper Triassic, Carnian, NE Italy). *Memorie di Scienze Geologiche Università di Padova* 47:125–133.
- Roghi, G., P. Gianolla, L. Minarelli, C. Pilati, and N. Preto. 2010. Palynological correlation of Carnian humid pulses throughout western Tethys. *Palaeogeography, Palaeoclimatology, Palaeoecology* 290:89–106.
- Rohlf, F. J. 2006. tpsDig, Version 2.10. Department of Ecology and Evolution, State University of New York, Stony Brook, NY.
- . 2007. tpsRelw, Version 1.45. Department of Ecology and Evolution, State University of New York, Stony Brook, NY.
- Rohlf, F. J., and L. F. Marcus. 1993. A revolution morphometrics. *Trends in Ecology and Evolution* 8:129–132.
- Schluter, D. 1996. Adaptive radiation along genetic lines of least resistance. *Evolution* 50:1766–1774.
- Siahsarvie, R. 2012. Comparaison de la divergence morphologique et génétique chez la souris domestique au cours de son expansion géographique. Ph.D. thesis. Université Montpellier 2. 56 p.
- Simms, M. J., and A. H. Ruffell. 1990. Climatic and biotic change in the late Triassic. *Journal of the Geological Society* 147:321–327.
- Stanley, G. D., Jr. 1988. The history of early Mesozoic reef communities: a three-step process. *Palaaios* 3:170–183.
- Sun, Y., M. M. Joachimski, P. B. Wignall, C. Yan, Y. Chen, H. Jiang, L. Wang, and X. Lai. 2012. Lethally hot temperatures during the Early Triassic greenhouse. *Science* 338:366–370.
- Thioulouse, J., and D. Chessel. 1987. Les analyses multitableaux en écologie factorielle. I: De la typologie d'état à la typologie de fonctionnement par l'analyse triadique. *Acta Oecologica Oecologia Generalis* 8:463–480.
- Tolmacheva, T., and A. Löfgren. 2000. Morphology and paleogeography of the Ordovician conodont *Paracordylodus gracilis* Lindström, 1955: comparison of two populations. *Journal of Paleontology* 74:1114–1121.
- Trotter, J. A., I. S. Williams, C. R. Barnes, C. Lécuyer, and R. S. Nicoll. 2008. Did cooling oceans trigger Ordovician biodiversification? Evidence from conodont thermometry. *Science* 321:550–554.
- Trotter, J. A., I. S. Williams, A. Nicora, M. Mazza, and M. Rigo. 2015. Long-term cycles of Triassic climate change: a new $\delta^{18}\text{O}$ record from conodont apatite. *Earth and Planetary Science Letters* 415:165–174.
- Urduy, S., L. A. Wilson, J. T. Haug, and M. R. Sánchez-Villagra. 2013. On the unique perspective of paleontology in the study of developmental evolution and biases. *Biological Theory* 8:293–311.
- Wainwright, P. C. 2007. Functional versus morphological diversity in macroevolution. *Annual Review of Ecology, Evolution, and Systematics* 38:381–401.
- Wenzel, B., C. Lécuyer, and M. M. Joachimski. 2000. Comparing calcite and phosphate oxygen isotope paleothermometers— $\delta^{18}\text{O}$ of Silurian brachiopods and conodonts. *Geochimica et Cosmochimica Acta* 64:1859–1872.
- Wickham, H. 2016. *Ggplot2: elegant graphics for data analysis*. Springer, New York.
- Wright, S. 1982. The shifting balance theory and macroevolution. *Annual Review of Genetics* 16:1–20.